ADVANCED OPTICAL MATERIALS
www.advopticalmat.de

Tunable Thermofluorochromic Sensors Based on Conjugated Polymers

Christian Bellacanzone, Jaume Ramon Otaegui, Jordi Hernando, Daniel Ruiz-Molina, and Claudio Roscini**

Even though thermofluorochromic materials are eternal candidates for their use in multiple applications, they are still limited as they require complex synthetic strategies to accomplish tunable optical properties and/or provide optical changes only over a very wide temperature range. By taking advantage of the high sensitivity of the optical properties of conjugated polymers and oligomers to the external environment, herein phase change material (PCM)-based thermofluorochromic mixtures are created, where the solid-to-liquid transition of the PCM host triggers a sharp fluorescence color change of the dispersed polymers/oligomers. Fluorophore conjugation length, concentration, and PCM nature can be used to vary the spectral properties of the resulting materials along the visible region, covering a large part of the CIE 1931 color space. For the preparation of functional devices, this behavior can be directly transferred to the solid state by soaking or printing cellulose papers with the obtained thermofluorochromic mixtures as well as by structuring them into solid lipid particles that can be dispersed within polymer matrices. The resulting materials show very promising features as thermal sensors and anticounterfeiting labels.

1. Introduction

Thermoresponsive optical materials are increasingly gaining interest in applications such as optical thermometers, diagnostic tools, optoelectronic devices, and anticounterfeiting markers, among others.[1–13] Specially relevant are those whose emission can be controlled with temperature, as luminescence can be detected remotely with highly sensitive and fast responsive techniques and offers time and spatial resolution at the macro- (e.g., luminescent labels) and nanoscale (e.g., fluorescence microscopy). Inherent thermofluorochromic materials involve thermoresponsive molecular dyes,[14–20] quantum dots, and lanthanide-doped nanoparticles,[21] conjugated polymers,[22] or polymorphic dyes.[23,24,25] Even though several reports of the materials are available nowadays, their wide range of temperature responses and limited tunability of the color emission and/or switching temperature still hamper their complete implementation in commercial applications.

This is the case of the solid films and particles of conjugated polymers,[26] exhibiting relevant thermochromic (e.g., polydiacetylene[27–31] and polythiophenes[3,32–37]) and thermofluorochromicc (e.g., poly(phenylenevinylene))[38–41] properties with good emission efficiencies in the visible range. Even so, their implementation in thermal sensors has yet to explode due to their gradual optical changes over very broad temperature ranges, mainly due to continuous variation of their conformation, aggregation degree, and/or crystalline phase with temperature affecting their effective conjugation length. On top of that, the fine-tuning of the emitted colors and switching temperature is intrinsically related to the chemical nature of the polymer so it requires time consuming and not cost-effective chemical modifications of the polymer backbone and/or the pending functional side groups.

Herein, we report a novel material design to accomplish highly tunable dual-color thermofluorochromism in a broad region of the 1931 CIE color space. On the one hand, we aim to employ conjugated polymers as emitters, which are emissive both in homogeneous solutions and in the aggregated state and, more importantly, show fluorescence properties that are highly dependent on the surrounding medium. On the other hand, we propose the use of phase change materials (PCM; e.g., polymers waxes) as thermally responsive surrounding matrices. Phase change media (e.g., polymers and paraffins) have already been used to develop thermofluorochromic materials, even for nonintrinsically thermoresponsive dyes or particles.[2,42–58] Paraffinic and nonparaffinic PCMs are of particular interest as their sharp and easily tunable solid–liquid

C. Bellacanzone, J. R. Otaegui, D. Ruiz-Molina, C. Roscini
Catalan Institute of Nanoscience and Nanotechnology (ICN2)
CSIC and The Barcelona Institute of Science and Technology (BIST)
Campus UAB, Bellaterra, Barcelona 08193, Spain
E-mail: dani.ruiz@icn2.cat; claudio.roscini@icn2.cat
J. R. Otaegui, J. Hernando
Departament de Química
Universitat Autònoma de Barcelona
Cerdanyola del Vallès 08193, Spain
The ORCID identification number(s) for the author(s) of this article can be found under https://doi.org/10.1002/adom.202102423.

DOI: 10.1002/adom.202102423

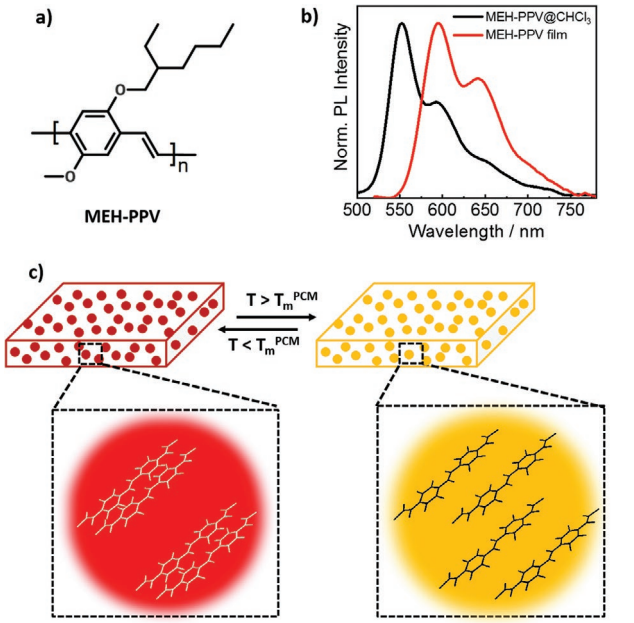

Figure 1. a) Molecular structure of MEH-PPV. b) Emission spectra of a $CHCl_3$ solution and a film of MEH-PPV. c) Scheme of a polymeric film loaded with solid lipid particles containing MEH-PPV chains. Depending on the solid or liquid state of the surrounding PCM, the MEH-PPV chains lie in their aggregated or nonaggregated forms within the particles, which provide different emission colors.

transition is a quite universal method to control the aggregation of the embedded fluorophores and their luminescence (e.g., by switching between monomeric and excimer emission upon dye aggregation).[59–68] Following this approach, up to now organic nonpolymeric PCMs have been successfully combined with small molecular fluorophores to yield single-color emission switching (off/on or on/off),[59,61,65] while multicolored thermal responses, with coarse color tunability, could only be accomplished by using different fluorescent molecules.[62,66,68] Although conjugated polymers are known to manifest highly medium-dependent emission properties, to our knowledge the only so far reported examples of PCM-based thermofluorochromism using a semiconductive polymer (polydiphenylacetylene) only provided a single-color on/off fluorescence modulation, and/or it required additional chemical functionalization to improve its miscibility with the surrounding PCM.[63,69]

As a proof-of-concept to validate our approach, we have selected the commercially available and broadly used fluorescent conjugated polymer poly[2-methoxy-5-(2-ethylhexyloxy)-1,4-phenylenevinylene (MEH-PPV, **Figure 1**a), as it shows three crucial characteristics required to achieve PCM-based thermofluorochromism. First, it strongly fluoresces in both homogeneous solutions (e.g., $\Phi_F^{toluene} = 0.34$)[70] and in the aggregated state (e.g., film, $\Phi_F^{film} = 0.10–0.15$).[71] Second, its luminescence is highly environment-dependent: i) diluted MEH-PPV liquid solutions (e.g., in $CHCl_3$) present a high energy emission band at $\lambda_{1,max} \approx 555$ nm and weaker shoulders at around $\lambda_2 \approx 600$ and $\lambda_3 \approx 655$ nm,[72–76] mainly arising from the 0–0, 0–1, and 0–2 vibronic progression of the $S_1 \rightarrow S_0$ transition of the single intrachain exciton emission (Figure 1b);[72] ii) MEH-PPV concentrated solutions, films and particles exhibit largely redshifted and broader emission spectra with bands at $\lambda_{max} \approx 600$ nm (and a weaker shoulder at 640 nm, Figure 1b), which are ascribed to polymer aggregates or other interchain species (e.g., exciplexes, charge-separated polaron pairs, etc.).[77–80] And third, shorter oligomeric species of different conjugation length and aggregation-dependent luminescence[45,56,57] can be used for a control of the fluorescence properties along the whole visible range, upon sonication of the parent MEH-PPV polymer.[81]

Beyond the bulk studies, these mixtures endorsed the preparation of thermofluorochromic papers or composite polymeric film (integrated as solid lipid particles, Figure 1c), to obtain thermal sensors over a large temperature range.

2. Results and Discussion

2.1. Switchable Fluorescence of MEH-PPV in PCM Mixtures

The 20-carbon inert paraffin eicosane (EC, melting point $T_m^{EC} = 36.5$ °C[82]), already used to thermally modulate the aggregation and therefore fluorescence of small molecular dyes,[59,60,64] was first chosen as a PCM in our work and mixed with 0.01 wt% MEH-PPV (**EC/MEH_0.01**, see the Supporting Information for experimental details). In the solid state (20 °C), the mixture showed a broad emission band at $\lambda_{max} = 603$ nm and a shoulder at 640 nm characteristic of the aggregated polymer (Figure S1, Supporting Information). Upon heating up to 60 °C, a little blueshift of the main luminescence band at $\lambda_{max} = 591$ nm and a more defined and less intense shoulder at $\lambda = 630$ nm were observed. This negligible change upon PCM melting was attributed to the low solubility of MEH-PPV in EC and the tendency of the polymer to aggregate in both its liquid and solid phases, as confirmed by the formation of polymer particles in suspension visible even by naked eye and the characteristic spectral features reported for MEH-PPV films or poor-solvent solutions where the polymer is predominantly in its aggregated state (Figure 1b).[70] Similar results were found in related paraffins such as hexadecane (HD, $T_m^{HD} = 18.2$ °C)[83] and tetradecane (TD, $T_m^{TD} = 5$ °C) (0.01 wt%, Figure S1, Supporting Information).[82]

To overcome this limitation we proposed the use of dodecanoic acid (DA, $T_m^{DA} = 43$ °C)[82] as a PCM, whose carboxylic acid functionality could enhance the MEH-PPV solubility, at least in the liquid state, through dipole–dipole interactions such as hydrogen bonds. Moreover, DA had already been used to modulate the optical performance of proton-sensitive organic photochromes[84] or yield reversible aggregation-induced quenching of fluorescent xanthene dyes.[65]

The emission spectrum of the solid mixture of MEH-PPV (0.1 wt%) in DA (**MEH/DA_0.1**), measured at 20 °C, showed the characteristic pattern of aggregated polymer species with a broad and intense band at $\lambda_{max} = 614$ nm and a shoulder at 650 nm (**Figure 2**a and **Table 1**). Above its melting point, a homogeneous liquid solution was obtained, without forming apparent macroscopic aggregates despite the 10-fold concentration increase used relative to the previous paraffin mixtures. The fluorescence spectrum of the molten solution showed a maximum at $\lambda_{max} = 595$ nm, a new high-energy band at

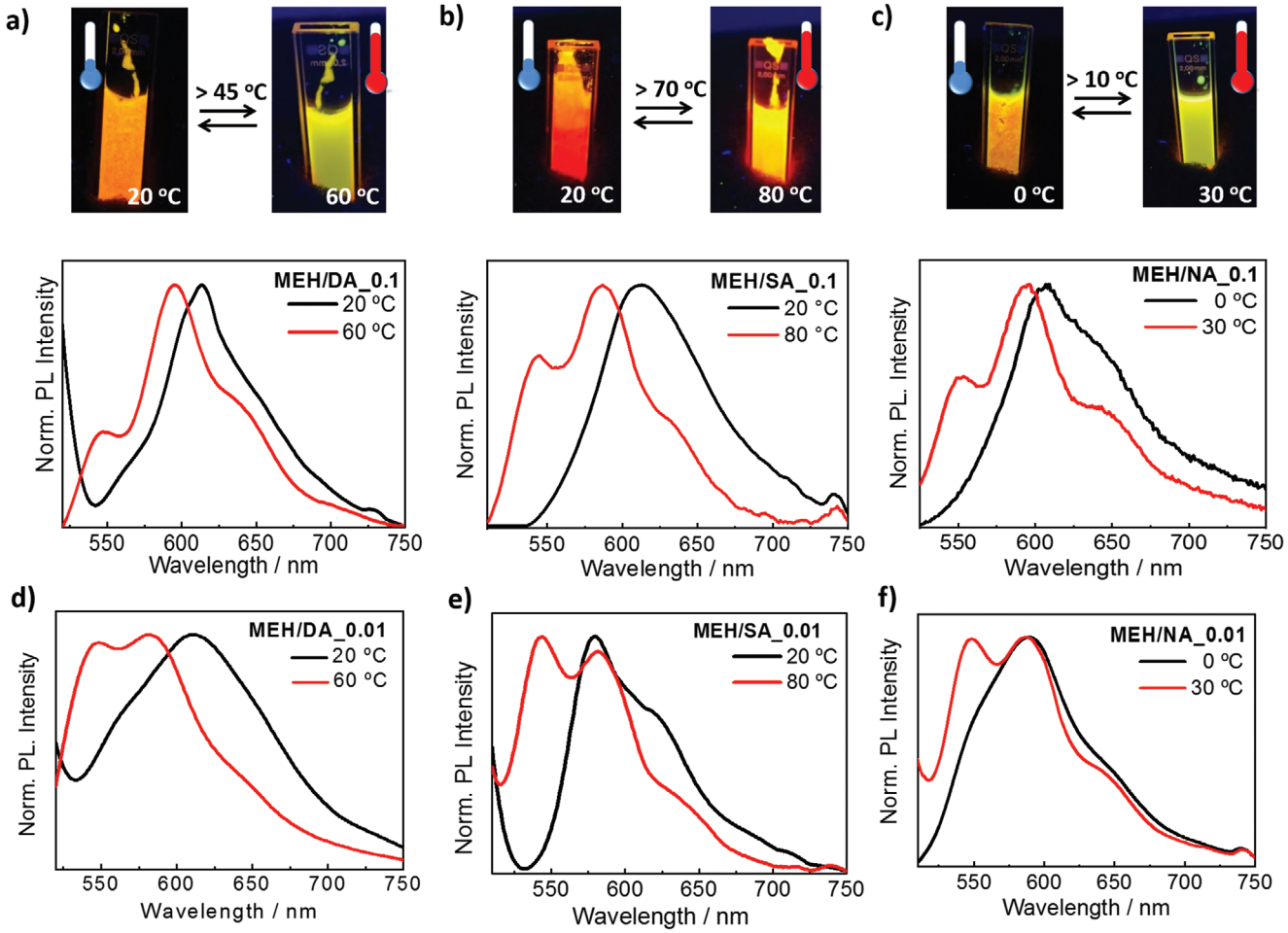

Figure 2. Images and normalized emission spectra of the a) **MEH/DA_0.1**, b) **MEH/SA_0.1**, and c) **MEH/NA_0.1** mixtures below and above their respective T_m^{PCM} under UV light (λ_{exc} = 365 nm). Normalized emission spectra of the d) **MEH/DA_0.01**, e) **MEH/SA_0.01**, and f) **MEH/NA_0.01** mixtures below and above their respective T_m^{PCM} under UV light (λ_{exc} = 365 nm).

λ_{max} = 546 nm and the low-intensity shoulder at λ_{max} = 634 nm. These features differed significantly from the emission spectrum of solid **MEH/DA_0.1** mixture and are reminiscent of the vibronic fluorescent bands of MEH-PPV in homogeneous organic solutions,[70] though with a different $I_{0\text{-}1}/I_{0\text{-}0}$ intensity band ratio that we ascribed to the remaining aggregated species in melted **MEH/DA_0.1** (Figure 2a and Table 1). Macroscopically, these aggregation changes resulted in a sharp (within 10 °C) emission color transition from orange to yellow observed by naked-eye (Figure 2a) –, i.e., thermofluorochromism.

To further corroborate the temperature-induced fluorescence modulation is caused by the polymer aggregation/redissolution in the solid/liquid PCM, we performed absorption and diffused reflectance spectra of the PCM mixture in its liquid and solid state, respectively (Figure S2, Supporting Information). Reflectance spectra were converted in F(R) functions through the Kubelka–Munk equation. Broad F(R) spectra with λ_{max} = 520–550 nm were obtained for the PCM solid mixture. Above the T_m^{PCM} the spectra blueshifted to λ_{max} = 490–500 nm and became narrower, approaching the λ_{max} position of the absorption spectrum of a homogeneous solution of MEH-PPV in $CHCl_3$ (Figure S2, Supporting Information). This strongly supports the formation of ground-state polymer (static) aggregates in the solid PCMs, though the further presence of dynamic aggregates cannot be excluded. The fact that the band of the liquid **MEH/DA_0.1** mixtures is broader than that of the $CHCl_3$ solution confirms that MEH-PPV aggregates are still present in the liquid DA, as previously showed by the emission spectra manifesting $I_{0\text{-}1}/I_{0\text{-}0}$ ratio different from those described for $CHCl_3$ homogeneous solutions.

Worth to mention is that the aggregation/disaggregation processes did not affect the emission efficiency, as demonstrated by the absolute fluorescence quantum yield values, which did not vary significantly when passing from the solid (Φ_F = 0.15) to the liquid (Φ_F = 0.19) state (Table 1). The slightly higher value registered for the liquid solution agrees with quantum yield data previously reported for MEH-PPV organic solutions and films.[70,71] This result, combined with the evident spectral changes observed upon melting the PCM, makes this system a good dual-color thermofluorochromic material. On top of that, these mixtures manifested quite good stability, as corroborated by the i) fluorescence quantum yield values in the solid (Φ_F = 0.15) and liquid (Φ_F = 0.18) state for the same mixture, measured 1 week later, which remained practically constant; and ii)

Table 1. Thermofluorochromic properties of the **MEH/DA**, **MEH/NA**, and **MEH/SA** mixtures: emission spectral maxima, $I_{0\text{-}1}/I_{0\text{-}0}$ intensity ratio for the liquid state, chromaticity coordinates, and absolute fluorescence quantum yield values.

Mixture	MEH-PPV conc. [wt%]	T [°C]	λ_1[a)] [nm]	λ_2[a)] [nm]	λ_3[a)] [nm]	$I_{0\text{-}1}/I_{0\text{-}0}$	1931 CIE coordinates (x,y)	Φ_F
MEH/DA	0.1	20	—	614	650	—	(0.605, 0.394)	0.15
		60	546	595	634	2.56	(0.550, 0.448)	0.19
	0.01	20	—	610	—	—	(0.539, 0.455)	0.16
		60	548	581	643	1.04	(0.469, 0.524)	0.19
MEH/NA	0.1	0	—	610	648	—	(0.599, 0.391)	0.17
		20	549	592	641	1.66	(0.526, 0.471)	0.19
	0.01	0	—	589	640	—	(0.513, 0.476)	0.27
		20	548	588	638	1.01	(0.475, 0.519)	0.35
MEH/SA	0.1	20	550	617	650	—	(0.616, 0.383)	0.17
		80	542	604	629	1.42	(0.485, 0.494)	0.19
	0.01	20	567	580	617	—	(0.529, 0.419)	0.18
		80	544	580	640	0.94	(0.453, 0.540)	0.17

[a)]For the monomeric emission in the molten mixtures, bands are assigned to vibronic transitions 0-0, 0-1, and 0-2.

reproducible thermal luminescence responses of the MEH-PPV/PCM mixtures upon repetitive heating/cooling cycles (Figure S3, Supporting Information).

The color transition temperature was successfully modulated using two analogous PCMs of strikingly different T_m, stearic acid (**MEH/SA_0.1**, $T_m^{SA} = 69.3$ °C)[82] and nonanoic acid (**MEH/NA_0.1**, $T_m^{NA} = 12.4$ °C),[82] and the same 0.1 wt% MEH-PPV concentration. The emission spectra of both mixtures in the solid state show broad unstructured emission bands at $\lambda_{max} = 617$ nm (**MEH/SA_0.1** at 20 °C) and $\lambda_{max} = 610$ nm (**MEH/NA_0.1** at 0 °C), with the former displaying a larger band broadening and redshift probably due to the lower solubility of MEH-PPV in the long-alkyl chain SA (Figure 2b,c and Table 1). An increase of the temperature over the melting point, up to 80 and 30 °C for **MEH/SA_0.1** and **MEH/NA_0.1**, respectively, induced a 18 and 13 nm hypsochromic shift of the main luminescence bands and the appearance of new high-energy bands corresponding to monomer emission at $\lambda_{max} = 542$ and 549 nm. Actually, the larger contribution of such high-energy bands relative to what observed for the **MEH/DA_0.1** mixture, was attributed to a larger degree of polymer disaggregation because of its enhanced solubility in short-alkyl chain NA and at the high temperature required to melt SA. Again the spectrally different emission observed in the solid and liquid state, showed similar efficiency in quantum yield experiments (Table 1).

Once more, the narrowing and blueshift of absorption spectra of the **MEH/SA_0.1** and **MEH/NA_0.1** upon melting confirmed the fluorescence spectral variations observed upon PCM transition are related to the aggregation/disaggregation processes (Figure S2, Supporting Information).

Finally, temperature-dependent fluorescence measurements obtained every 10 °C over a large thermal range for the low- (**MEH/NA_0.1**) and high-T_m (**MEH/SA_0.1**) mixtures revealed negligible spectral changes once below or above the PCM melting point, corroborating that the thermally-induced optical changes are triggered by the PCM solid-to-liquid transition (Figure S4, Supporting Information),[85] occurring, in all cases, within 10 °C.

The reversible thermofluorochromic properties of MEH-PPV in aliphatic carboxylic acids were preserved upon 10-fold dilution of the polymer content (0.01 wt%, Figure 2d–f and Table 1; and Figure S5, Supporting Information), though with some differences. In the solid state, all the mixtures (**MEH/NA_0.01**, **MEH/SA_0.01**, and **MEH/DA_0.01**) showed a blueshift of the broad emission band (λ_{max} ≈580–610 nm) compared to the more concentrated samples, probably due to lower aggregation effects. For the same reason, the liquid diluted mixtures presented larger relative intensities of the high-energy band at λ_{max} ≈550 nm related to intrachain emission (see $I_{0\text{-}1}/I_{0\text{-}0}$, Table 1). Absolute quantum yield values of the solid and liquid mixtures were also comparable and slightly higher than those of the more concentrated mixtures, possibly due to a decrease of ground-state aggregates that are more prone to undergo excited state relaxation through nonradiative decays. This conclusion was supported by the F(R) spectra measured for the diluted mixtures, which displayed narrower and blueshifted (λ_{max} = 500–520 nm) bands than the corresponding concentrated solutions, thus further suggesting a lower degree of aggregation or the formation of smaller aggregates (Figure S6, Supporting Information). Also in this case, the melted solutions displayed a blueshift of the respective absorption bands (λ_{max} = 480–490 nm), which was associated to the redissolution of the polymer molecules, as it happens in homogeneous $CHCl_3$ solution. Overall, this allowed obtaining concentration-dependent thermally-induced optical changes, where the switching colors of the solid and liquid mixtures were displaced toward the yellow region of the CIE 1931 color space upon dilution of the MEH-PPV/PCM mixture, i.e., fine tuning of the thermofluorochromic behavior without the need of varying the fluorophore of choice (Table 1; and Figure S7, Supporting Information).

2.2. Switchable Fluorescence of Oligomers in PCM Mixtures

To further generalize this approach, we also prepared PCM mixtures with shorter oligomeric species straightforwardly

obtained from MEH-PPV through a sonochemical strategy already reported by us (see the Supporting Information for details).[81] Applying this methodology, we synthesized three different types of MEH-PPV oligomers, which we named **MEH-4**, **MEH-2**, and **MEH-1.5** in decreasing order of polymer length. Interestingly, such oligomers exhibit different emission and absorption properties due to the modification of the effective conjugation length (Figure S8, Supporting Information), which particularly decreased from that of the untreated polymer (n_{ECL} = 10–17) to n_{ECL} = 2 for the shorter oligomers.[81]

The solid mixtures of **MEH-4** in DA at 0.1 wt% (**MEH-4/DA_0.1**) and 0.01 wt% (**MEH-4/DA_0.01**) showed concentration-dependent fluorescence with broad and nonstructured emission bands centered at λ_{max} = 581 (orange emission color) and 571 nm (green emission color), respectively (**Figure 3**a,b and **Table 2**). Heating above the DA melting point induced a 43 and 48 nm blueshift of the emission band of the **MEH-4/DA_0.1** (λ_{max} = 538 nm) and **MEH-4/DA_0.01** (λ_{max} = 523 nm) liquid mixtures, respectively. The fluorescence quantum yield values of the oligomer mixtures did not vary significantly passing from the solid (0.14 and 0.21 for **MEH-4/DA_0.1** and **MEH-4/DA_0.01** samples, respectively) to the liquid state (0.19, 0.30), confirming that these oligomer mixtures could also be used as dual-color thermofluorochromic materials. In addition, the reduction of oligomer concentration also yielded higher emission quantum yield values in both solid and liquid mixtures, probably due to a decrease in the degree of aggregation. As exemplified by **MEH-4/DA_0.1**, the emission switch took place within a narrow temperature range of 10 °C around T_m^{DA} (Figure S9a, Supporting Information) and was fully reversible upon several heating/cooling cycles (Figure S9b, Supporting Information). Further tuning of the emission color was obtained with the use of the **MEH-2/DA_0.1** (0.1 wt%) and **MEH-2/DA_0.01** (0.01 wt%) mixtures, which presented fluorescence maxima at λ_{max} = 550 and 539 nm in the solid state (Φ_F = 0.02 and 0.04), respectively, that are blueshifted by almost 30 nm in comparison with **MEH-4/DA** samples. Moreover, these values were further blueshifted by 45 and 34 nm, respectively, upon melting at 50 °C (Φ_F = 0.04 for both concentrations), thus demonstrating that the thermofluorochromic behavior was preserved even when decreasing nECL (Table 2; and Figure S10, Supporting Information). The band maxima of the F(R) spectra of the solid DA mixtures were broader and/or more redshifted than the absorption bands of the liquid solutions, which again evidences the formation of the aggregates of the MEH-PPV oligomers in the solid PCM, especially at higher concentrations (Figure S11, Supporting Information). Finally, the fair agreement between the absorption spectrum of the liquid DA mixtures with those of MEH-4 and MEH-2 in $CHCl_3$ suggests the good redissolution of these oligomers in the liquid PCM (Figure S11, Supporting Information).

As for the **MEH-1.5** oligomer, experiments were conducted in this case in NA to tune the solid–liquid transition down to 12.4 °C. At 0.1 wt% concentration, the **MEH-1.5/NA** mixture (**MEH-1.5/NA_0.1**) provided a further blueshifted thermoresponsive switching upon melting (from λ_{max} = 495 to 478 nm, Figure S12a, Supporting Information). However, this was not observed for **MEH-1.5/NA_0.01** with a 10-fold decrease in emitter concentration, which showed similar spectra in both the solid and liquid phases (λ_{max} ≈475 nm). This result was ascribed to the increased solubility of the shorter **MEH-1.5** oligomer and higher solvation capability of NA compared to DA, thus leading to well dispersed **MEH-1.5** molecules showing intrachain emission even in the solid state of the sample upon dilution (Table 2; and Figure S12b, Supporting Information).

2.3. Modification of the PCM Nature

The larger solubility of **MEH-4** in organic media with respect to the parent MEH-PPV polymer also allowed us to use paraffins as host PCM matrices to accomplish thermofluorochromic materials. **MEH-4** was thus dissolved in EC at different concentrations, obtaining **MEH-4/EC_0.1** (0.1 wt%) and **MEH-4/EC_0.01** (0.01 wt%) mixtures. The first remarkable feature found for these samples was the ≈20 nm emission blueshift registered for the solid **MEH-4/EC_0.01** mixture with respect to its DA counterpart, revealing an intrinsic matrix-induced solvatochromic effect prior to any thermal treatment. In addition, they showed the characteristic thermal switching behavior previously observed in long alkyl chain carboxylic acids, with 46 nm (**MEH-4/EC_0.1**) and 33 nm (**MEH-4/EC_0.01**) blueshifts upon heating above T_m^{EC} (Figure 3c and Table 2; and Figure S13a, Supporting Information).

When the same **MEH-4** oligomer was dissolved at 0.1 wt% concentration in HD (T_m^{HD} = 18.2 °C),[82] the resulting **MEH-4/HD_0.1** mixture also displayed two main characteristics: i) a 33 nm fluorescence switch upon melting from λ_{max} = 560 to λ_{max} = 527 nm (Figure 3d), and ii) a slightly blueshift of the band maxima of the solid and liquid mixtures compared to the corresponding EC solution. On the other hand, the less concentrated **MEH-4/HD_0.01** solution displayed negligible thermofluorochromism, probably due to the higher solubility of the oligomer in solid HD that yielded the blueshifted monomer emission in both phases of the PCM (Table 2; and Figure S13b, Supporting Information).

From these results, we can infer that the nature of the PCM critically determines the performance of the thermofluorochromic mixtures with conjugated polymers and oligomers as it allows both fine tuning of the switching temperature and emission response, and modulation of the position of the emission bands owing to solvatochromism. Such tunability can be further increased, by varying the emitter conjugation length and concentration, as illustrated for the different MEH-PPV polymer and oligomer samples analyzed. Altogether, this enables a controlled and broad variation of the thermofluorochromic behavior of the materials developed herein along the CIE 1931 color space, as shown in Figure 3e.

2.4. Cellulose-Based Temperature Sensors

Once proven the efficiency of our strategy toward thermofluorochromism based on conjugated polymers and PCMs, we aimed to integrate these mixtures into solid substrates to develop easy-to-handle sensor devices. The substrate of choice for this was cellulose paper, a cheap, biodegradable, and fully-scalable material that has been rediscovered for the fabrication of added-value

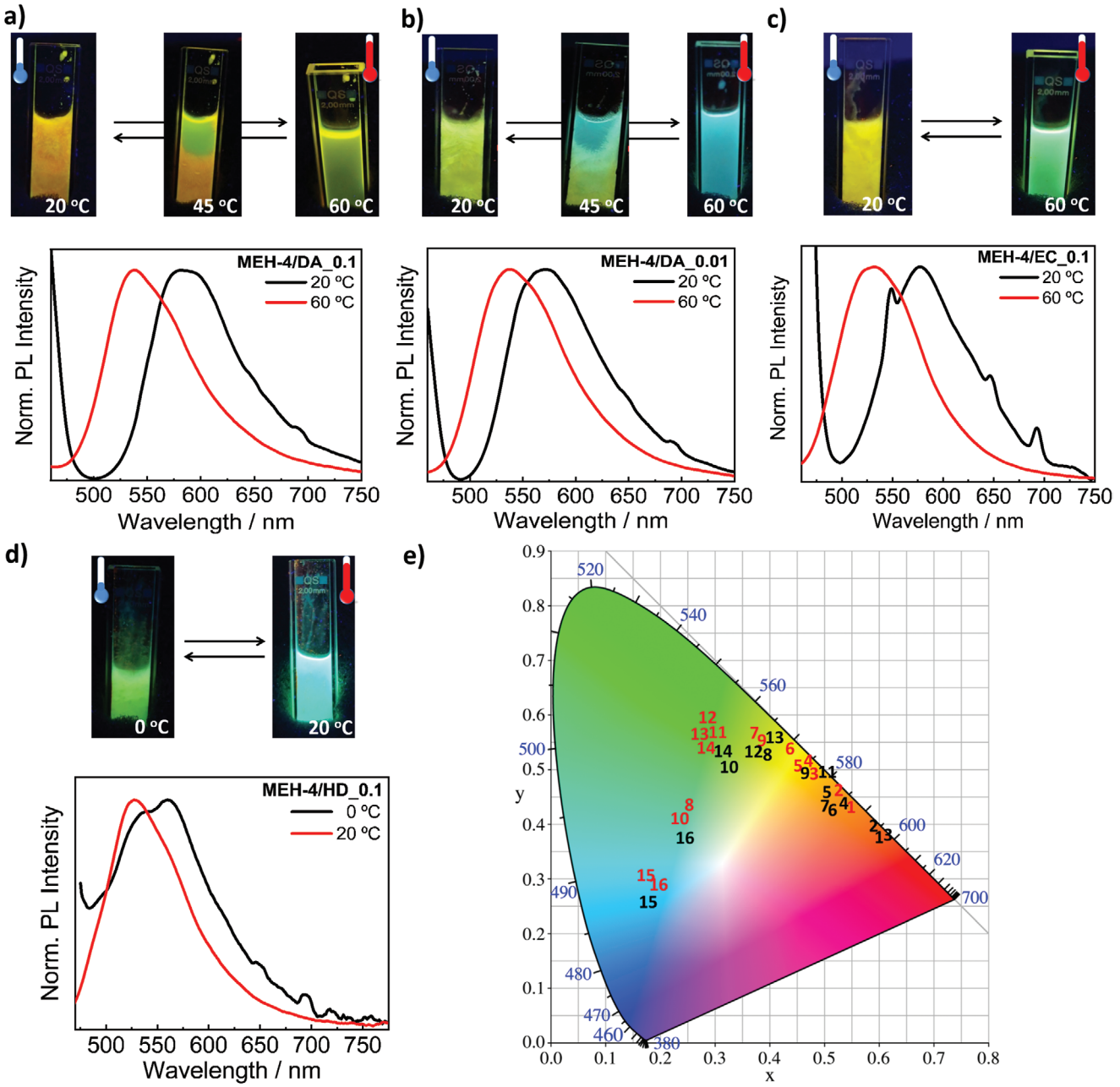

Figure 3. a,b) Images and normalized emission spectra of a) **MEH-4/DA_0.1** and b) **MEH-4/DA_0.01** before and after PCM melting (λ_{exc} = 365 nm). The pictures of the cuvettes at 45 °C show the still incomplete solid-to-liquid transition of the PCM mixtures with clearly fractioned emitted colors: the bottom part, still solid, presents the corresponding initial emissions, while the top one, already melted, clearly displays the luminescence of the final liquid mixtures. c,d) Images and normalized emission spectra of c) **MEH-4/EC_0.1** and d) **MEH-4/HD_0.1** below and above the respective T_m^{PCM} under UV light (λ_{exc} = 365 nm). e) 1931 CIE chromaticity coordinates of the emission color of the following mixtures below and above their T_m^{PCM}. 1: **MEH/DA_0.1**; 2: **MEH/NA_0.1**; 3: **MEH/SA_0.1**; 4: **MEH/DA_0.01**; 5: **MEH/NA_0.01**; 6: **MEH/SA_0.01**; 7: **MEH-4/DA_0.1**; 8: **MEH-2/DA_0.1**; 9: **MEH-4/DA_0.01**; 10: **MEH-2/DA_0.01**; 11: **MEH-4/EC_0.1**; 12: **MEH-4/HD_0.1**; 13: **MEH-4/EC_0.01**; 14: **MEH-4/HD_0.01**; 15: **MEH-1.5/NA_0.1**; 16: **MEH-4/NA_0.01**. The chromaticity coordinates for the solid and melted samples are shown in black and red, respectively.

sensors, i.e., the so called smart papers.[86] As a proof of concept, we prepared four different cellulose papers by soaking them with melted **MEH/SA_0.1**, **MEH/DA_0.01**, **MEH/NA_0.1**, and **MEH-4/EC_0.1** mixtures, which were selected according to their rich and differential emission and interconversion temperature. Afterward, the systems were cooled down to 0 °C to allow for PCM solidification. Interestingly, the resulting smart papers retained the colors and switching behavior around the respective T_m^{PCM} of the corresponding bulk mixtures (**Figure 4**a), though slight discrepancies in emission color and/or color contrast were observed that can be attributed to a variety of factors, e.g., the distinct thicknesses of the papers and

Table 2. Thermofluorochromic properties of the mixtures of MEH-PPV oligomers with PCMs: emission spectral maxima below and above their T_m^{PCM}, emission spectral shifts upon heating and emission chromaticity coordinates.

Mixture	Oligomer conc. [wt%]	Temperature [°C]	λ_{max} [nm]	Spectral shift [nm]	1931 CIE coordinates (x,y)
MEH-4/DA	0.1	20	581	43	(0.535, 0.463)
		60	538		(0.389, 0.573)
	0.01	20	571	48	(0.484, 0.509)
		60	523		(0.380, 0.574)
MEH-2/DA	0.1	20	550	45	(0.419, 0.533)
		60	505		(0.260, 0.439)
	0.01	20	539	34	(0.351, 0.512)
		60	505		(0.250, 0.425)
MEH-1.5/NA	0.1	0	495	17	(0.260, 0.384)
		20	478		(0.201, 0.292)
	0.01	0	476	1	(0.197, 0.275)
		20	475		(0.201, 0.304)
MEH-4/EC	0.1	20	578	46	(0.494, 0.500)
		60	532		(0.336, 0.578)
	0.01	20	554	33	(0.412, 0.558)
		60	521		(0.301, 0.591)
MEH-4/HD	0.1	0	560	33	(0.392, 0.542)
		20	527		(0.340, 0.580)
	0.01	0	523	2	(0.333, 0.545)
		20	521		(0.323, 0.551)

bulk mixtures, where excitation light can also penetrate differently and lead to differential contributions of the reabsorption processes to the final colors emitted; the non-negligible autofluorescence of the cellulose substrates used; or the migration of a small percentage of MEH-PPV polymers/oligomers toward the cellulose fibers of the papers, which will be no longer affected by PCM melting. In spite of this, the clear and large thermofluorochromic responses registered for the free-standing papers

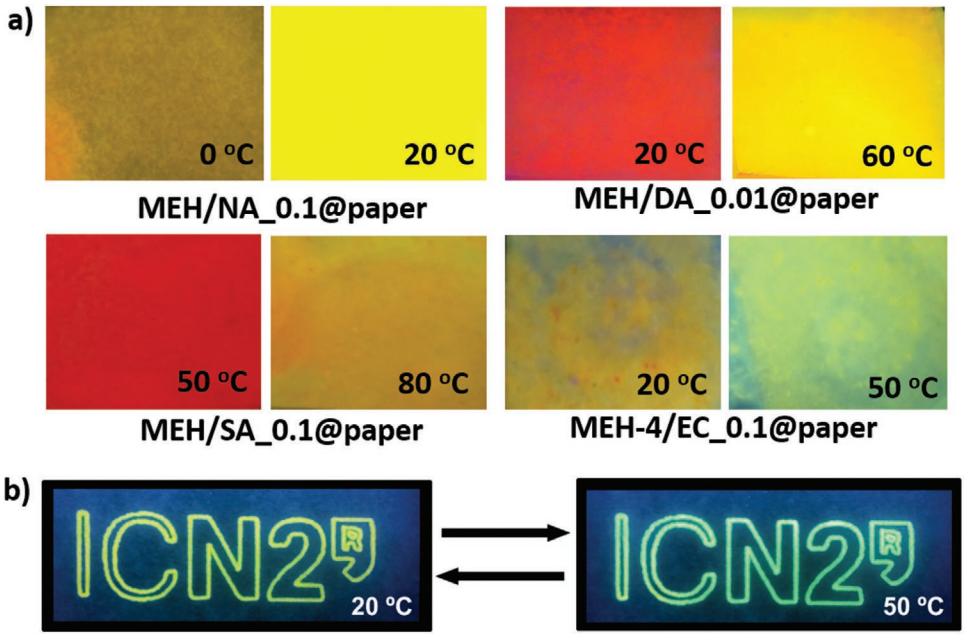

Figure 4. a) Cellulose papers soaked with the **MEH/NA_0.1**, **MEH/DA_0.01**, **MEH/SA_0.1**, **MEH-4/EC_0.1** mixtures, whose emission below and above their T_m^{PCM} is shown (λ_{exc} = 365 nm). b) Emission of a cellulose paper wax-printed with the **MEH-2/DA_0.1** mixture, below and above the T_m^{DA}. The background blue emission is due to the cellulose paper autofluorescence.

prepared make them usable as temperature sensing platforms that are accessible through a simple and scalable approach. In addition, though the price of commercially available conjugated polymers such as MEH-PPV might be often high, the little amount required for the fabrication of these smart papers (typically, 16 mg cm^{-2}) makes them also of low cost.

On a further step, even more complex thermoresponsive fluorescent patterns were created on cellulose papers by wax-printing the desired MEH-PPV/PCM using a plotter with an attached pen, which was coated with aluminum foil and connected to a power supply to induce Joule heating. With this, we were able to print well-resolved thermoresponsive fluorescent writings and patterns by using the **MEH-2/DA_0.1** mixture, which modified its emission color upon reaching the T_m^{DA} (Figure 4b). Noticeably, the resolution of the drawings was preserved even after several heating-cooling cycles, thus indicating the good encapsulation of the PCM mixtures within the cellulose fibers.

2.5. Microstructuration and Integration into Free-Standing Films for Temperature Sensing

Beyond smart papers, we aimed to explore the incorporation of MEH-PPV/PCM mixtures into free-standing polymeric films that are highly suitable for the preparation of optical temperature sensing devices. However, this is not as simple as in the case of cellulose papers, since polymeric films are not porous and therefore do not adsorb the thermofluorochromic mixtures. On the other hand, the direct mixing of MEH/PCM solutions with matrix polymers would alter the final composition and, as a result, their emission switching properties. For all this, we then structured the MEH/PCM mixtures into solid lipid microparticles (SLMs) that can be easily dispersed within inert polymer films, following a similar approach already used in our group with core–shell microcapsules,[10,87–89] liquid nanodroplets,[90] and solid lipid nanoparticles[91] to preserve the optical properties of macroscopic solutions in solid composites.

First of all, SLMs were prepared from the representative **MEH/DA_0.1** and **MEH/SA_0.1** mixtures through the emulsion-cooling method (see the Supporting Information for more details). SEM and optical microscopy images of the obtained **MEH/DA_SLMs** (**Figure 5**a,b) and **MEH/SA_SLMs** (Figure 5c; and Figure S14, Supporting Information) confirmed the successful formation of the particles (diameter ≈10–50 µm). Moreover, the red spots observed in the core of the microparticles by optical microscopy suggest the successful encapsulation of the MEH-PPV polymer. Accordingly, both SLMs undergo the fluorescence switch observed in bulk once they are heated above the T_m^{PCM}, with the blueshift of the main band and the formation of the high energy band at 547 nm (Figure 5d; and Figure S15, Supporting Information). However, some differences of the emission spectra are observed compared to the measurements of the bulk mixtures. This was ascribed to the partial loss of the polymer during the SLMs preparation, which caused the reduction of the polymer final concentration in the structured PCM. Next, the SLMs were incorporated into a hydrophilic poly(vinyl alcohol) (PVA) polymer matrix, which is not miscible with the liquid and solid phases of the SLMs. This was achieved upon drop casting a colloidal dispersion of **MEH@DA_SLMs** in an aqueous PVA solution and allowing the water to evaporate (see the Supporting Information).

The presence of phase-separated **MEH@DA_SLMs** embedded within the PVA layer was confirmed by differential scanning calorimetry (DSC), where we clearly observed the signal arising from DA solid–liquid transition at $T \approx 44$ °C (Figure S16, Supporting Information). This guarantees that the microparticles remain confined within the resulting **MEH@DA@PVA** free-standing film, thereby retaining the thermally-induced fluorescence modulation of the bulk MEH-PPV/DA mixtures (Figure 5e,f).

To illustrate the applicability of the composite films prepared, one of them was used to successfully sense the temperature of an aqueous solution heated at 60 °C. As shown in Figure 5g, the fraction of the film that was not submerged in the solution remained at room temperature and, consequently, exhibited the red-orange emission arising from **MEH@DA_SLMs** in the solid state; by contrast, the part of the polymer layer immersed into the heated sample experienced the phase transition of the embedded **MEH@DA_SLMs** and, therefore, the corresponding switch to yellow colored fluorescence.

3. Conclusions

In summary, herein we have reported a straightforward and general strategy to obtain sharply changing dual-color fluorescent thermoresponsive systems based on the semiconductive polymer MEH-PPV dissolved in phase change materials. The thermally-induced emission switch of these mixtures is fully reversible and relates to the different environment generated around the fluorophores during the solid–liquid transition of the PCM: large aggregates emitting at lower energies are formed in the solid state while non-/less aggregated systems with higher energy emission are generated in the liquid PCM phase. Therefore, the PCM matrix assures the control and tunability of the transition temperature, as well as guarantees a sharp (within 10 °C) thermal switching behavior for the conjugated polymer emission, which to date had only been showed to display progressive thermofluorochromic changes over wide temperature ranges.

Noticeably, by taking advantage of the very high sensitivity of conjugated polymer molecules to the external environment, our strategy enables fine modulation of the color and magnitude of the thermofluorochromic response by simply controlling the fluorophore concentration and/or the PCM type. In addition, the color palette of these thermoresponsive fluorescent switching materials can be further expanded with MEH-PPV oligomers to other regions of the CIE 1931 chromaticity diagram without the need for the tedious synthesis or functionalization of alternative fluorophores. Noticeably, the MEH-PPV/PCM mixtures can be easily transferred to cellulose papers for the development of paper-based color-changing temperature sensors. Furthermore, they are also suitable for wax-printing, which opens the door for the preparation of patterns of interest for sensing and anticounterfeiting labels. Finally, our PCM-based materials can be structured as solid lipid microparticles, which upon incorporation into polymeric

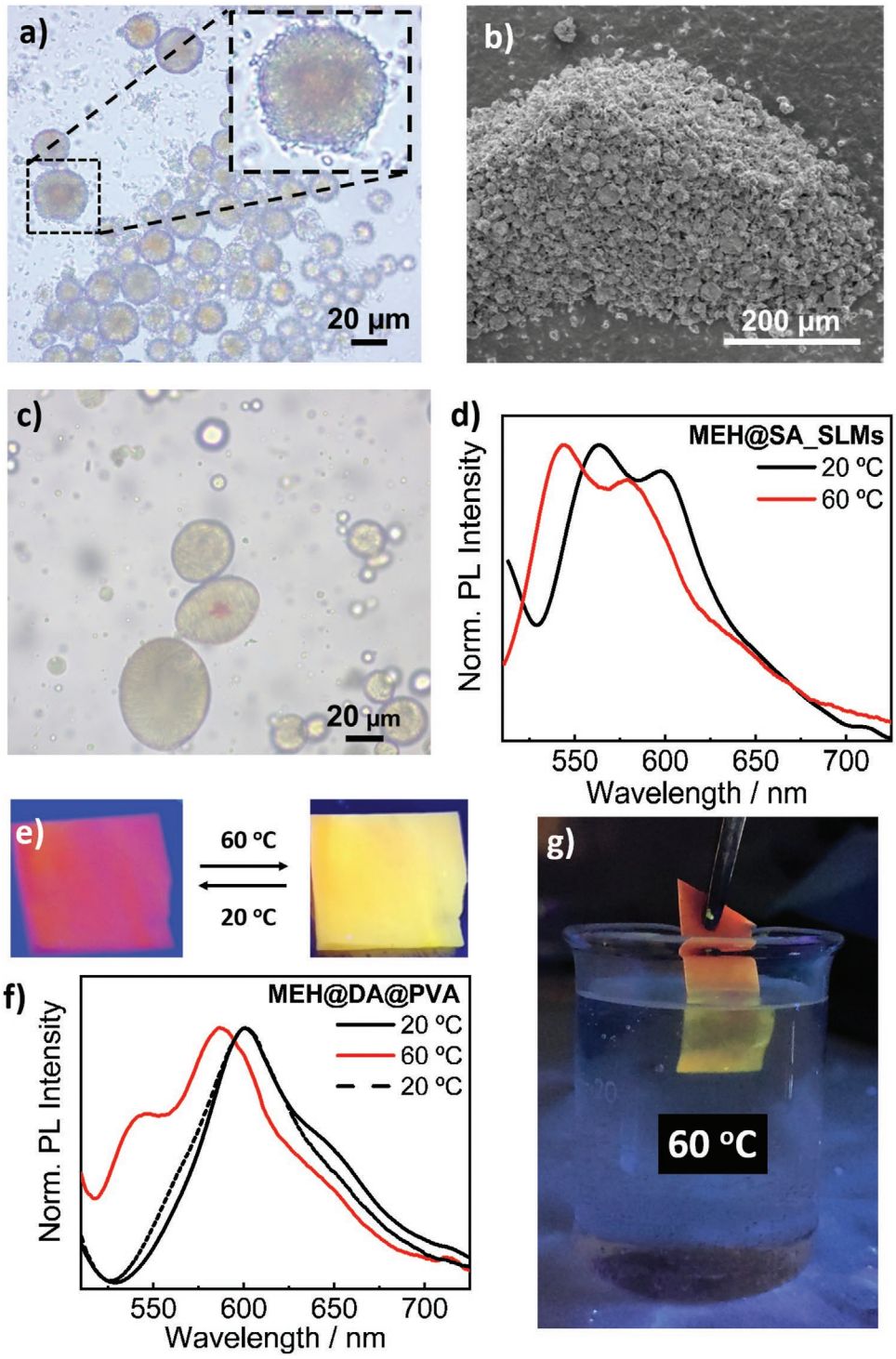

Figure 5. a) Optical microscopy and b) SEM images of **MEH@DA_SLMs**. c) Optical microscopy image and d) temperature-dependent emission spectra of **MEH@SA_SLMs**. e) Image (λ_{exc} = 365 nm) and f) temperature-dependent emission spectra of a **MEH@DA@PVA** film. g) Demonstration of the use of the **MEH@DA@PVA** film as a fluorescent temperature sensor (λ_{exc} = 365 nm).

matrices enable obtaining free-standing films with thermofluorochromic behavior that could be directly used as temperature sensors.

Supporting Information

Supporting Information is available from the Wiley Online Library or from the author.

Acknowledgements

This work was supported by Grant Nos. RTI2018-098027-B-C21 and PID2019-106171RB-100 funded by No. MCIN/AEI/10.13039/501100011033 and by ERDF A way of making Europe. The ICN2 is funded by the CERCA programme/Generalitat de Catalunya. The ICN2 is supported by the Severo Ochoa Centres of Excellence programme, Grant No. SEV-2017-0706 funded by No. MCIN/AEI/10.13039/501100011033. This work was also supported by Generalitat de Catalunya (No. 2017 SGR00465 project). J.R.O. aknowledge the Generalitat de Catalunya (AGAUR) for his predoctoral FI fellowship.

Conflict of Interest

The authors declare no conflict of interest.

Data Availability Statement

Research data are not shared.

Keywords

aggregation, conjugated polymers, fluorescence, phase-change materials, sensors, thermofluorochromism

Received: November 8, 2021
Revised: February 14, 2022
Published online: March 20, 2022

[1] A. Seeboth, D. Lötzsch, *Thermochromic Phenomena in Polymers*, Smithers Rapra, Shawbury, UK **2008**.
[2] A. Seeboth, D. Lötzsch, R. Ruhmann, O. Muehling, *Chem. Rev.* **2014**, *114*, 3037.
[3] M. Leclerc, *Adv. Mater.* **1999**, *11*, 1491.
[4] X. Wang, O. S. Wolfbeis, R. J. Meier, *Chem. Soc. Rev.* **2013**, *42*, 7834.
[5] J. Zhou, B. del Rosal, D. Jaque, S. Uchiyama, D. Jin, *Nat. Methods* **2020**, *17*, 967.
[6] A. Kishimura, T. Yamashita, K. Yamaguchi, T. Aida, *Nat. Mater.* **2005**, *4*, 546.
[7] S. Hirata, K.-S. Lee, T. Watanabe, *Adv. Funct. Mater.* **2008**, *18*, 2869.
[8] K. Ogasawara, K. Nakamura, N. Kobayashi, *J. Mater. Chem. C* **2016**, *4*, 4805.
[9] W. Ren, G. Lin, C. Clarke, J. Zhou, D. Jin, *Adv. Mater.* **2020**, *32*, 1901430.
[10] N. A. Vázquez-Mera, J. R. Otaegui, R. S. Sánchez, G. Prats, G. Guirado, D. Ruiz-Molina, C. Roscini, J. Hernando, *ACS Appl. Mater. Interfaces* **2019**, *11*, 17751.
[11] A. Abdollahi, H. Roghani-Mamaqani, B. Razavi, M. S. Kalajahi, *ACS Nano* **2020**, *14*, 14417.
[12] Y. Ma, Y. Dong, S. Liu, P. She, J. Lu, S. Liu, W. Huang, Q. Zhao, *Adv. Opt. Mater.* **2020**, *8*, 1901687.
[13] C. Baleizão, S. Nagl, S. Borisov, M. Schäferling, O. Wolfbeis, M. Berberan-Santos, *Chem. – Eur. J.* **2007**, *13*, 3643.
[14] J. Feng, L. Xiong, S. Wang, S. Li, Y. Li, G. Yang, *Adv. Funct. Mater.* **2013**, *23*, 340.
[15] J. Feng, K. Tian, D. Hu, S. Wang, S. Li, Y. Zeng, Y. Li, G. Yang, *Angew. Chem., Int. Ed.* **2011**, *50*, 8072.
[16] Z. Xie, C. Chen, S. Xu, J. Li, Y. Zhang, S. Liu, J. Xu, Z. Chi, *Angew. Chem, IntEd* **2015**, *54*, 7181.
[17] D. Li, W. Hu, J. Wang, Q. Zhang, X.-M. Cao, X. Ma, H. Tian, *Chem. Sci.* **2018**, *9*, 5709.
[18] J. Wang, N. Wang, G. Wu, S. Wang, X. Li, *Angew. Chem., Int. Ed.* **2019**, *58*, 3082.
[19] Y. Cao, J. K. Nagle, M. O. Wolf, B. O. Patrick, *J. Am. Chem. Soc.* **2015**, *137*, 4888.
[20] L. Liu, X. Wang, N. Wang, T. Peng, S. Wang, *Angew. Chem., Int. Ed.* **2017**, *56*, 9160.
[21] B. del Rosal, E. Ximendes, U. Rocha, D. Jaque, *Adv. Opt. Mater.* **2017**, *5*, 1600508.
[22] J.-Y. Lin, B. Liu, M.-N. Yu, X.-H. Wang, L.-B. Bai, Y.-M. Han, C.-J. Ou, L.-H. Xie, F. Liu, W.-S. Zhu, X.-W. Zhang, H.-F. Ling, P. N. Stavrinou, J.-P. Wang, D. D. C. Bradley, W. Huang, *J. Mater. Chem. C* **2018**, *6*, 1535.
[23] Z. Q. Yao, J. Xu, B. Zou, Z. Hu, K. Wang, Y. J. Yuan, Y. P. Chen, R. Feng, J. B. Xiong, J. Hao, X. H. Bu, *Angew. Chem., Int. Ed.* **2019**, *58*, 5614.
[24] B. Prusti, P. Sarkar, S. K. Pati, M. Chakravarty, *J. Mater. Chem. C* **2021**, *9*, 9555.
[25] B. Prusti, P. K. Samanta, N. J. English, M. Chakravarty, *Chem. Commun.* **2021**,*57*, 12321.
[26] M. S. Vezie, S. Few, I. Meager, G. Pieridou, B. Dörling, R. S. Ashraf, A. R. Goñi, H. Bronstein, I. McCulloch, S. C. Hayes, M. Campoy-Quiles, J. Nelson, *Nat. Mater.* **2016**, *15*, 746.
[27] D. J. Ahn, E.-H. Chae, G. S. Lee, H.-Y. Shim, T.-E. Chang, K.-D. Ahn, J.-M. Kim, *J. Am. Chem. Soc.* **2003**, *125*, 8976.
[28] Z. Yuan, C.-W. Lee, S.-H. Lee, *Angew. Chem.* **2004**, *116*, 4293.
[29] Y. Gu, W. Cao, L. Zhu, D. Chen, M. Jiang, *Macromolecules* **2008**, *41*, 2299.
[30] D. J. Ahn, S. Lee, J.-M. Kim, *Adv. Funct. Mater.* **2009**, *19*, 1483.
[31] L. Yu, S. L. Hsu, *Macromolecules* **2012**, *45*, 420.
[32] K. Tashiro, K. Ono, Y. Minagawa, M. Kobayashi, T. Kawai, K. Yoshino, *J. Polym. Sci., Part B: Polym. Phys.* **1991**, *29*, 1223.
[33] C. Roux, M. Leclerc, *Chem. Mater.* **1994**, *6*, 620.
[34] M. Ahlskog, J. Paloheimo, H. Stubb, P. Dyreklev, M. Fahlman, O. Inganäs, M. R. Andersson, *J. Appl. Phys.* **1994**, *76*, 893.
[35] M. Leclerc, K. Faid, *Adv. Mater.* **1997**, *9*, 1087.
[36] F. Raymond, N. Di Césare, M. Belletête, G. Durocher, M. Leclerc, *Adv. Mater.* **1998**, *10*, 599.
[37] N. Kurokawa, H. Yoshikawa, N. Hirota, K. Hyodo, H. Masuhara, *ChemPhysChem* **2004**, *5*, 1609.
[38] R. Jakubiak, M. Yan, W. C. Wan, B. R. Hsieh, L. J. Rothberga, *Isr. J. Chem.* **2000**, *40*, 153.
[39] F. A. C. Oliveira, L. A. Cury, A. Righi, R. L. Moreira, P. S. S. Guimarães, F. M. Matinaga, M. A. Pimenta, R. A. Nogueira, *J. Chem. Phys.* **2003**, *119*, 9777.
[40] G. Wantz, L. Hirsch, N. Huby, L. Vignau, A. S. Barrière, J. P. Parneix, *J. Appl. Phys.* **2005**, *97*, 034505.
[41] A. Köhler, S. T. Hoffmann, H. Bässler, *J. Am. Chem. Soc.* **2012**, *134*, 11594.
[42] F. Azizian, A. J. Field, B. M. Heron, C. Kilner, *Chem. Commun.* **2012**, *48*, 750.
[43] S. M. Burkinshaw, J. Griffiths, A. D. Towns, *J. Mater. Chem.* **1998**, *8*, 2677.
[44] M. A. White, M. LeBlanc, *J. Chem. Educ.* **1999**, *76*, 1201.
[45] M. Kinami, B. R. Crenshaw, C. Weder, *Chem. Mater.* **2006**, *18*, 946.
[46] B. R. Crenshaw, C. Weder, *Adv. Mater.* **2005**, *17*, 1471.
[47] C. E. Sing, J. Kunzelman, C. Weder, *J. Mater. Chem.* **2009**, *19*, 104.
[48] J. Kunzelman, B. R. Crenshaw, M. Kinami, C. Weder, *Macromol. Rapid Commun.* **2006**, *27*, 1981.
[49] C. J. Ellison, J. M. Torkelson, *J. Polym. Sci. B: Polym. Phys.* **2002**, *40*, 2745.
[50] O. van den Berg, W. G. F. Sengers, W. F. Jager, S. J. Picken, M. Wübbenhorst, *Macromolecules* **2004**, *37*, 2460.
[51] B.-S. Lee, H.-S. Shin, *Food Sci. Biotechnol.* **2012**, *21*, 1483.

[52] T. Corrales, C. Abrísci, C. Peinado, F. Catalina, *Macromolecules* **2004**, *37*, 6596.
[53] A. Pucci, F. Signori, R. Bizzarri, S. Bronco, G. Ruggeri, F. Ciardelli, *J. Mater. Chem.* **2010**, *20*, 5843.
[54] B. R. Crenshaw, J. Kunzelman, C. E. Sing, C. Ander, C. Weder, *Macromol. Chem. Phys.* **2007**, *208*, 572.
[55] N. Chandrasekharan, L. A. Kelly, *J. Am. Chem. Soc.* **2001**, *123*, 9898.
[56] K. K. Kartha, S. S. Babu, S. Srinivasan, A. Ajayaghosh, *J. Am. Chem. Soc.* **2012**, *134*, 4834.
[57] A. Ajayaghosh, S. J. George, *J. Am. Chem. Soc.* **2001**, *123*, 5148.
[58] X. Liu, S. Li, J. Feng, Y. Li, G. Yang, *Chem. Commun.* **2014**, *50*, 2778.
[59] J. R. Otaegui, P. Rubirola, D. Ruiz-Molina, J. Hernando, C. Roscini, *Adv. Opt. Mater.* **2020**, *8*, 2001063.
[60] G. Massaro, G. Zampini, D. Ruiz-Molina, J. Hernando, C. Roscini, L. Latterini, *J. Phys. Chem. C* **2019**, *123*, 4632.
[61] W. Zhang, X. Ji, B.-J. Peng, S. Che, F. Ge, W. Liu, M. Al-Hashimi, C. Wang, L. Fang, *Adv. Funct. Mater.* **2020**, *30*, 1906463.
[62] J. Du, L. Sheng, Q. Chen, Y. Xu, W. Li, X. Wang, M. Li, S. X. Zhang, *Mater. Horiz.* **2019**, *6*, 1654.
[63] Y. J. Jin, R. Dogra, I. W. Cheong, G. Kwak, *ACS Appl. Mater. Interfaces* **2015**, *7*, 14485.
[64] G. Massaro, J. Hernando, D. Ruiz-Molina, C. Roscini, L. Latterini, *Chem. Mater.* **2016**, *28*, 738.
[65] A. Julià López, D. Ruiz-Molina, K. Landfester, M. B. Bannwarth, C. Roscini, *Adv. Funct. Mater.* **2018**, *28*, 1801492.
[66] J. Du, L. Sheng, Y. Xu, Q. Chen, C. Gu, M. Li, S. X.-A. Zhang, *Adv. Mater.* **2021**, *33*, 2008055.
[67] H. Liu, W. Song, X. Chen, J. Mei, Z. Zhang, J. Su, *Mater. Chem. Front* **2021**, *5*, 2294.
[68] R. Liao, S. Gu, X. Wang, X. Zhang, X. Xie, H. Sun, W. Huang, *J. Mater. Chem. C* **2020**, *8*, 8430.
[69] Y.-J. Jin, B. Shin-Il Kim, W.-E. Lee, C.-L. Lee, H. Kim, K.-H. Song, S.-Y. Jang, G. Kwak, *NPG Asia Mater.* **2014**, *6*, e137.
[70] C. J. Collison, L. J. Rothberg, V. Treemaneekarn, L. Yi, *Macromolecules* **2001**, *34*, 2346.
[71] N. C. Greenham, I. D. W. Samuel, G. R. Hayes, R. T. Phillips, Y. A. R. R. Kessener, S. C. Moratti, A. B. Holmes, R. H. Friend, *Chem. Phys. Lett.* **1995**, *241*, 89.
[72] S. Wang, J. W. Ryan, A. Singh, J. G. Beirne, E. Palomares, G. Redmond, *Langmuir* **2016**, *32*, 329.
[73] R. Chang, J. H. Hsu, W. S. Fann, K. K. Liang, C. H. Chang, M. Hayashi, J. Yu, S. H. Lin, E. C. Chang, K. R. Chuang, S. A. Chen, *Chem. Phys. Lett.* **2000**, *317*, 142.
[74] H. Zhang, X. Lu, Y. Li, X. Ai, X. Zhang, G. Yang, *J. Photochem. Photobiol., A* **2002**, *147*, 15.
[75] R. F. Cossiello, M. D. Susman, P. F. Aramend, T. D. Z. Atvars, *J. Lumin.* **2010**, *130*, 415.
[76] S. T. Hoffmann, H. Bässler, A. Köhler, *J. Phys. Chem. B* **2010**, *114*, 17037.
[77] T.-Q. Nguyen, V. Doan, B. J. Schwartz, *J. Chem. Phys.* **1999**, *110*, 4068.
[78] T.-Q. Nguyen, I. B. Martini, J. Liu, B. J. Schwartz, *J. Phys. Chem. B* **2000**, *104*, 237.
[79] R. D. Schaller, L. F. Lee, J. C. Johnson, L. H. Haber, R. J. Saykally, *J. Phys. Chem. B* **2002**, *106*, 9496.
[80] M. A. T. da Silva, I. F. L. Dias, J. L. Duarte, E. Laureto, I. Silvestre, L. A. Cury, P. S. S. Guimarães, *J. Chem. Phys.* **2008**, *128*, 094902.
[81] C. Bellacanzone, C. Roscini, M. C. Ruiz Delgado, R. P. Ortiz, D. Ruiz-Molina, *Part. Part. Syst. Charact.* **2018**, *35*, 1700322.
[82] W. Haynes, *CRC Handbook of Chemistry and Physics*, CRC Press, Boca Raton, FL **2014**.
[83] H. L. Finke, M. E. Gross, G. Waddington, H. M. Huffman, *J. Am. Chem. Soc.* **1954**, *76*, 333.
[84] A. Julià López, J. Hernando, D. Ruiz-Molina, P. González-Monje, J. Sedó, C. Roscini, *Angew. Chem., Int. Ed.* **2016**, *55*, 15044.
[85] The fact that the largest change is verified at 80 °C instead of 70 °C (the T_m^{SA} = 69.3 °C) was ascribed to the difference between the set and real temperature of the sample holder.
[86] H. Nawaz, X. Zhang, S. Chen, T. You, F. Xu, *Carbohydr. Polym.* **2021**, *267*, 118135.
[87] N. Vázquez-Mera, C. Roscini, J. Hernando, D. Ruiz-Molina, *Adv. Opt. Mater.* **2013**, *1*, 631.
[88] N. A. Vázquez-Mera, C. Roscini, J. Hernando, D. Ruiz-Molina, *Adv. Funct. Mater.* **2015**, *25*, 4129.
[89] A. Julià-López, D. Ruiz-Molina, J. Hernando, C. Roscini, *ACS Appl. Mater. Interfaces* **2019**, *11*, 11884.
[90] H. Torres Pierna, D. Ruiz-Molina, C. Roscini, *Mater. Horiz.* **2020**, *7*, 2749.
[91] J. R. Otaegui, D. Ruiz-Molina, L. Latterini, J. Hernando, C. Roscini, *Mater. Horiz.* **2021**, *8*, 3043.